steel research international

Austenite Evolution and Solute Partitioning during Thermal Cycling in the Intercritical Range of a Medium-Mn Steel

Maria-Ioanna Tzini, Panagiota Sarafoglou, Andreas Stieben, Gregory Haidemenopoulos,* and Wolfgang Bleck

The evolution of austenite fraction and the associated solute partitioning during the intercritical annealing of medium-Mn steels are of great importance for austenite stabilization and the mechanical performance of this class of steels. In the present work, a 4.5Mn steel is subjected to a cyclic treatment and the evolution of the austenite fraction is measured with dilatometry. The evolution of austenite fraction and solute partitioning are simulated for a case where the starting time of the cyclic treatment is well before the equilibrium fractions have been established in the respective isothermal intercritical treatment. The evolution of austenite during thermal cycling in the intercritical range comprises of forward, inverse, and stagnant stages. The fraction of austenite formed decreases in each successive cycle while the kinetics of the evolution of austenite is controlled by the Mn diffusion in ferrite. Partitioning of Mn and C takes place from ferrite to austenite during the cyclic transformation. Due to the low diffusivity in austenite, wells form in the composition profiles in austenite of both Mn and C. These wells are the locus of the interfacial compositions of austenite, corresponding to the variation of the local equilibrium conditions during the thermal cycle.

1. Introduction

Intercritical annealing is one of the main links of the process chain of medium-Mn steels. These steels belong to the third generation advanced high-strength steels, and contain 3–12 mass% manganese. Partitioning of manganese and carbon to the austenite, during intercritical annealing, stabilizes the austenitic phase. Transformation-induced plasticity (TRIP) of the retained austenite provides excellent combination of strength and ductility.[1–4] The role of retained austenite and especially its fraction and stability have long been identified as of paramount importance in exhibiting beneficial TRIP effects.[5–6] Thus, the understanding of the kinetics of partitioning in medium-Mn steel during intercritical annealing is a prerequisite to the design of medium-Mn steels. The topic is currently under intense investigation.[7–13] Cyclic partial phase transformation in the intercritical range has been employed recently to study the growth kinetics and phase transformations in low-Mn and low-C Fe–C–Mn alloys.[14–15] The procedure of thermal cycling in the intercritical range was also applied to investigate austenite growth kinetics in medium-Mn steels.[16] The strategy behind the modeling of cyclic intercritical annealing is that it allows to investigate the growth kinetics without the modeling uncertainties of nucleation being part of the transformation.[15] With this type of modeling, it is possible to accurately describe the interfacial conditions and more importantly the solute partitioning during the $\alpha \rightarrow \gamma$ and $\gamma \rightarrow \alpha$ transformations. In the above works, an "inverse" transformation stage as well as a "stagnant" stage were identified, in addition to the forward transformation of ferrite to austenite. The inverse transformation is defined as the transformation where the α/γ interface proceeds in a direction opposite to the temperature change, i.e., austenite forms during the cooling part of the cycle. During the stagnant stage the transformation is very sluggish, and proceeds at infinitesimal rate. In addition, it was shown[16] that the cyclic behavior depends on the starting time of the cyclic treatment relative to the isothermal transformation curve. So if the starting time is well after thermodynamic equilibrium has been established, hysteresis loops form in the volume fraction

[*] Prof. G. Haidemenopoulos, M.-I. Tzini, Dr. P. Sarafoglou
Department of Mechanical Engineering, University of Thessaly, Volos 38334, Greece
Email: hgreg@mie.uth.gr
A. Stieben, Prof. W. Bleck
Steel Institute, RWTH-Aachen University, Germany

DOI: 10.1002/srin.201600050

austenite versus temperature curve. On the other hand if the starting time is before the final phase equilibrium, then there is no formation of hysteresis loops and the evolution of the austenite volume fraction is characterized by an extended inverse transformation during the cooling part of the cycle. The aim of the present study is to study in more detail the inverse transformation stage and more specifically the solute partitioning which takes place during such cyclic transformations, especially for the case where the starting time of the cyclic treatment is well before thermodynamic equilibrium has been established in the respective isothermal intercritical annealing treatments.

The study is performed by simulating the cyclic transformations in the intercritical range. The experimental validation of austenite growth kinetics was performed with dilatometric techniques.

2. Materials and Methods

The material investigated was a medium-Mn steel with composition 0.2C–4.5Mn–0.15Si–0.1Cr–0.028Al (mass%). In order to define the maximum and minimum temperatures of the thermal cycle, an isopleth section at 4.5Mn was constructed with the Thermo-Calc software using the TCFE6 database,[17] shown in **Figure 1**. The cyclic thermal treatment for the study is depicted in **Figure 2** and the various characteristics of the cycle are given in **Table 1**. The cyclic thermal treatment consists of an isothermal holding at T_{is} and three cycles with temperature range between T_{max} and T_{min}. The cycle starts with heating at T_{is}, isothermal holding at this temperature for 2412 s followed by temperature cycling between T_{max} and T_{min}. The cycling ends with an isothermal holding for 1800s and

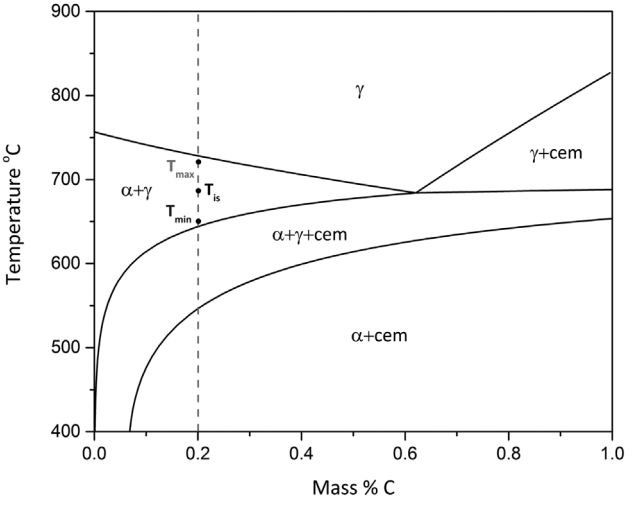

Figure 1. Isopleth section of the steel for the composition 4.5Mn–0.15Si–0.1Cr–0.028Al (mass%). The range of thermal cycling in the intercritical range ($\alpha+\gamma$) is indicated.

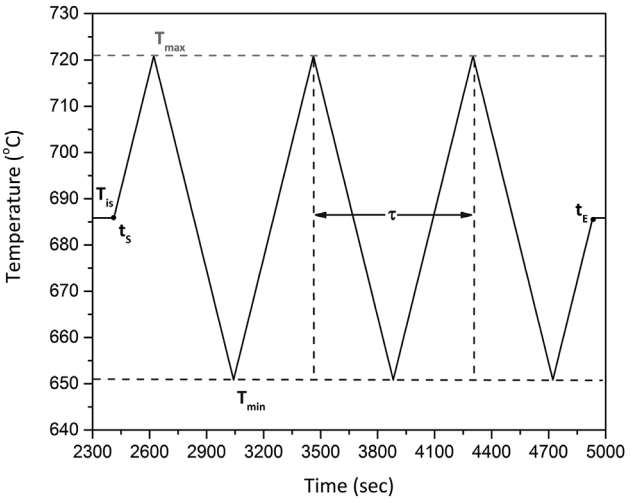

Figure 2. The thermal cycle used in the experiments and the simulation. T_{is} denotes the isothermal holding temperature, while T_{max} and T_{min} are the maximum and minimum temperatures of the cycle, respectively. The period of the cycle is τ. Time t_S corresponds to the start and time t_E to the end of the cyclic transformation.

cooling to ambient temperature. The values T_{is}, T_{max}, and T_{min} were specifically chosen to span the entire range of the $\alpha+\gamma$ region of the phase diagram. The heating and cooling rates (HR and CR) were kept constant for the three periods (τ) of the cycle. The equilibrium volume fractions of austenite (f_γ) and ferrite (f_α) at T_{is} are shown in the Table 1, as well. The austenite formation and associated solute partitioning during intercritical annealing were simulated with the DICTRA software[18] using the MOBFE2 mobility database for ferrous alloys. A single-cell planar geometry was employed, shown in **Figure 3**. Following the procedure established in a previous work,[7] a small region size was considered, equal to 1.085 μm, since it was anticipated that the interface movements during the cyclic transformation were going to be small. In addition, the solute partitioning is taking place at a small distance from the α/γ interface during the cyclic transformation. A thin austenite slice, 3.5 nm, was attached to the left of the ferrite region. The two regions were discretized with a linear grid consisting of 150 grid points. The initial compositions of the austenite slice and ferrite region were taken equal to the nominal compositions of the alloy. Although the compositions in the two phases are identical, the respective activities are not. Diffusional fluxes are generated between the two phases in response to the different activities. Zero flux boundary conditions (closed system) for all elements were imposed at the lower and upper boundaries of the system. The parameters monitored were the position of the α/γ interface, which when normalized to the total region size, corresponds to the austenite volume fraction, and the velocity of the α/γ interface (VOI). In addition to monitoring the α/γ interface position and velocity, the solute partitioning between the two phases was monitored.

Steel	A_1 [°C]	A_3 [°C]	T_{is} [°C]	T_{min} [°C]	T_{max} [°C]	ΔT [°C]	HR, CR [°C min^{-1}]	τ [s]	f_α [%]	f_γ [%]
Fe–0.2C–4.5Mn	644	728	686	651	721	70	10	840	0.394	0.605

Table 1. The characteristics of the thermal cycle. T_{is} is the isothermal holding temperature, T_{min} and T_{max} are the minimum and maximum temperatures, respectively, HR and CR are the heating and cooling rates, respectively, τ is the period of the cycle. The equilibrium volume fractions of ferrite and austenite at T_{is} are f_γ and f_α, respectively.

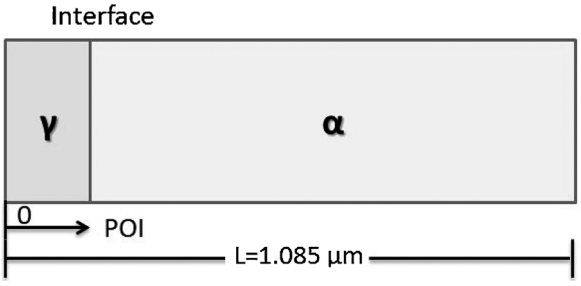

Figure 3. The calculation domain (cell) employed in the simulations for the cyclic transformation. POI denotes the position of the γ/α interface.

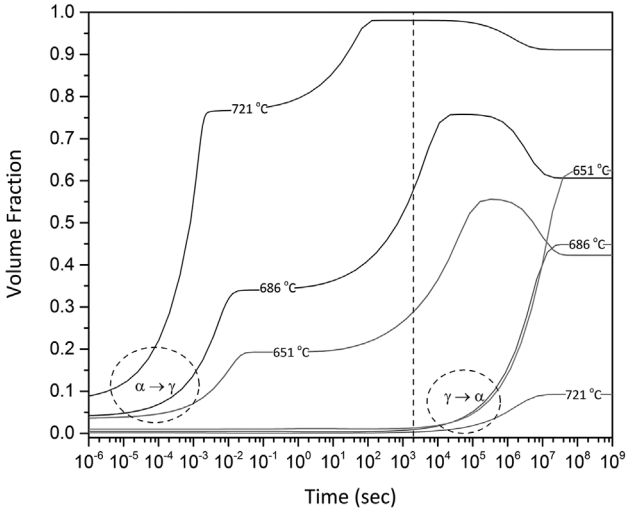

Figure 4. Evolution of the volume fraction of austenite and ferrite for the isothermal $\alpha \rightarrow \gamma$ and $\gamma \rightarrow \alpha$ transformations, respectively, in the Fe–0.2C–4.5Mn steel for temperatures 651, 686, and 721 °C. The dotted line denotes the starting time $t_s = 2412$ s of the cyclic transformation.

For the dilatometric measurements, the steel was prepared as an 80 kg ingot with a cross-section of $140 \times 140\,mm^2$ in a vacuum induction melting furnace (2 kHz). The ingots homogenized for 3 h at 1200 °C and open die forged to a cross-section of $60 \times 60\,mm^2$. After the forging process, the bars were air cooled to ambient temperature. Before the cyclic thermal treatment, samples with size of $25 \times 40 \times 40\,mm^3$, were austenitized in a salt bath at 950 °C for 1800s and quenched in oil. Thermal cycling was performed in the dilatometer according to the schedule of Figure 2. The dilatometer used was a BÄHR DIL805A dilatometer. The specimen used for dilatometry was a solid plate with dimensions $7 \times 4 \times 1.3\,mm^3$. The volume fraction of austenite was determined by the relative length change by subtracting the linear length change, which is attributed to thermal expansion and contraction.

3. Results and Discussion

3.1. Evolution of Austenite Fraction and Experimental Validation

The isothermal $\alpha \rightarrow \gamma$ and $\gamma \rightarrow \alpha$ transformations in the Fe–0.2C–4.5Mn steel are depicted in **Figure 4** for three temperatures 651, 686, 721 °C corresponding to the T_{min}, T_{is}, and T_{max} of the respective cyclic treatment. The evolution of austenite volume fraction during intercritical annealing takes place in three stages.[7,19,20] In stage I, non-partitioning local equilibrium (NPLE) growth of austenite takes place at short times and is controlled by carbon diffusion in ferrite. In stage II, partitioning local equilibrium (PLE) growth of austenite is controlled by manganese diffusion in ferrite, while in stage III, the PLE shrinkage of austenite is controlled by manganese diffusion in austenite. Compared to the $\gamma \rightarrow \alpha$, the $\alpha \rightarrow \gamma$ transformation is considerably faster. The dotted line in Figure 4 indicates the starting time (t_s) of the cyclic transformation after the isothermal holding. Following the applied thermal cycle in the dilatometric experiments, a starting time $t_s = 2412$s was selected. It can be deduced from Figure 4 that at this time the $\alpha \rightarrow \gamma$ transformation is still evolving, while the $\gamma \rightarrow \alpha$ transformation is very sluggish. The evolution of the austenite volume fraction f_γ versus temperature during thermal cycling is depicted in **Figure 5**. Points S and E on the volume fraction curve correspond to the start and the end of the cyclic transformation, respectively. Points A, B, and C correspond to T_{min} (651 °C), whereas points 1, 2, and 3 correspond to T_{max} (721 °C). It is observed that the interface does not change direction and the volume fraction is continuously increasing. The parts S-1, A-2, B-3, and C-E on the volume fraction curve correspond to the "forward" transformation where the f_γ is evolving with the temperature rise. Accordingly, the parts 1-A, 2-B, and 3-C′ correspond to the "inverse" transformation, where the interface proceeds

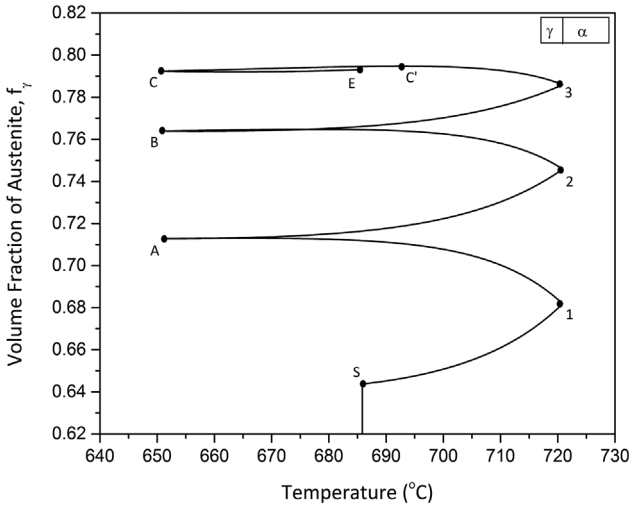

Figure 5. Evolution of austenite volume fraction during thermal cycling in the intercritical range.

in a direction opposite to the temperature change, i.e., austenite is forming during the cooling part of the cycle. Only part C′-C corresponds to a forward transformation, since a small decrease of the f_γ is detected with a decrease in temperature. It is interesting to see that the fraction of austenite formed decreases in each successive cycle. The fractions of austenite formed are 0.07, 0.05, and 0.03 in the first, second, and third cycles, respectively. In order to explain this behavior, the volume fraction of austenite f_γ, the temperature, and the velocity of the interface (VOI) versus time are depicted in **Figure 6**. The maxima in the VOI curve correspond to T_{max} while the minima correspond to T_{min}. The VOI decreases in each cycle and this leads to a lower amount of austenite forming in each cycle. The austenite volume fraction curve (f_γ) indicates that each cycle comprises of a forward transformation during heating, an inverse transformation during cooling, and a stagnant transformation stage. During the forward transformation, austenite grows as the temperature increases from the minimum to the maximum value of the cycle. At the same time, the velocity of the interface increases. During the inverse transformation, austenite continues to form during the cooling part of the cycle, while at the same time the velocity of the interface decreases. The transition between the forward and inverse transformations takes place at T_{max} where VOI is maximized. At the minimum temperature of the cycle where practically VOI = 0, the transformation is sluggish, corresponding to the stagnant transformation stage. Because at the selected time for the start of the cyclic transformation ($t_s = 2412$s), the rate of the $\gamma \rightarrow \alpha$ transformation is negligible compared to the rate of the $\alpha \rightarrow \gamma$ transformation, austenite formation during the cooling part of the cycle proceeds entirely by the inverse transformation. However, the VOI values in **Figure 7**a indicate that both transformations, forward and inverse, take place at comparable rates.

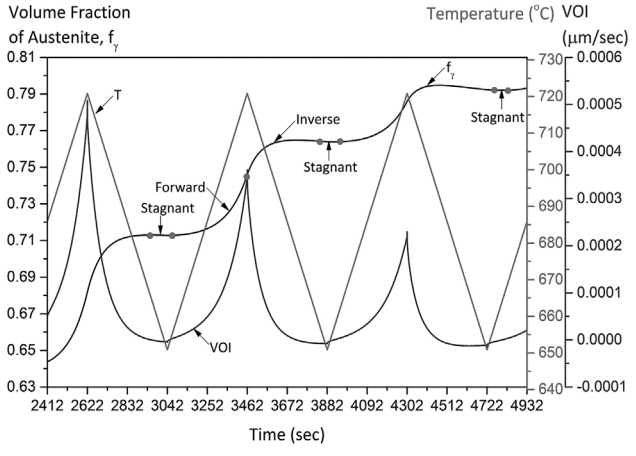

Figure 6. Evolution of austenite volume fraction (f_γ) and velocity of the γ/α interface (VOI) versus time during thermal cycling in the intercritical range. The forward, inverse, and stagnant transformation stages are indicated.

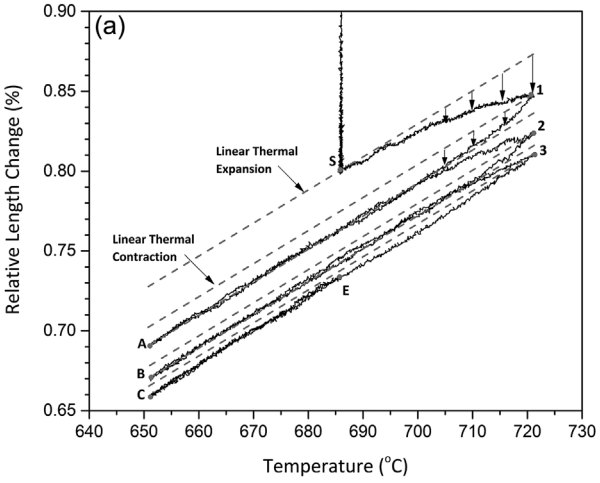

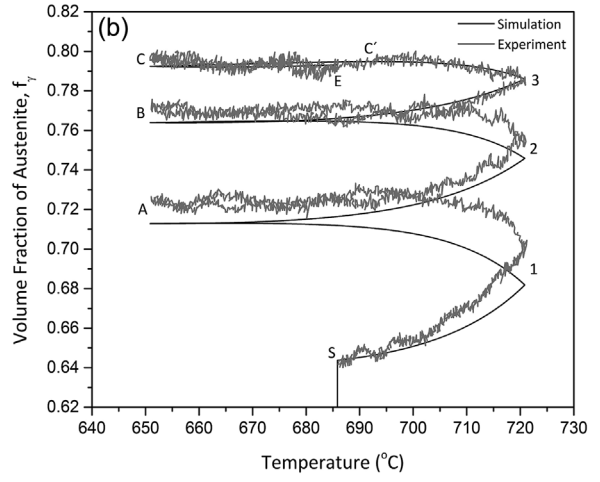

Figure 7. Dilatometry curves: a) relative length change versus T, b) fraction austenite versus T (comparison between dilatometry and simulation).

The dilatometric curve obtained from thermal cycling in the dilatometer is shown in Figure 7a. The relative length change is plotted versus temperature. From this curve, the volume fraction austenite is obtained by subtracting the linear thermal expansion and contraction during heating and cooling, respectively. This is depicted by the arrows from the dotted lines to the dilatometric curve. The result is shown in Figure 7b, together with the simulation result of Figure 6. The agreement between simulation and experiment is considered good. It appears that the simulation can describe the evolution of the austenite volume fraction during cyclic transformations in the intercritical range.

3.2. Solute Partitioning

The experimental validation of the simulation regarding the evolution of the austenite volume fraction allows to apply the method in order to simulate the evolution of solute partitioning during the cyclic transformation.

The evolution of the Mn profile during the first cycle is depicted in **Figure 8**a–d, where Figure 8a corresponds to the start of the cycle at T_{is} (686 °C), Figure 8b corresponds to T_{max} (721 °C), Figure 8c corresponds to T_{is} (686 °C), and Figure 8d corresponds to T_{min} (651 °C). During heating, between T_{is} and T_{max}, austenite forms by forward transformation. The Mn concentration of austenite at the α/γ interface decreases leaving a peak at point 1, as shown in Figure 8b. Points 2 and 3 in Figure 8b correspond to the Mn compositions of austenite and ferrite at the interface at T_{max} according to the local equilibrium conditions. Thus, the built-up of the Mn profile in austenite during heating from T_{is} to T_{max} corresponds to the line between points 1 and 2 in Figure 8b. During cooling from T_{max} to the intermediate temperature T_{is} and then to T_{min}, shown in Figure 8c and d, the inverse transformation takes place and the interface continues to

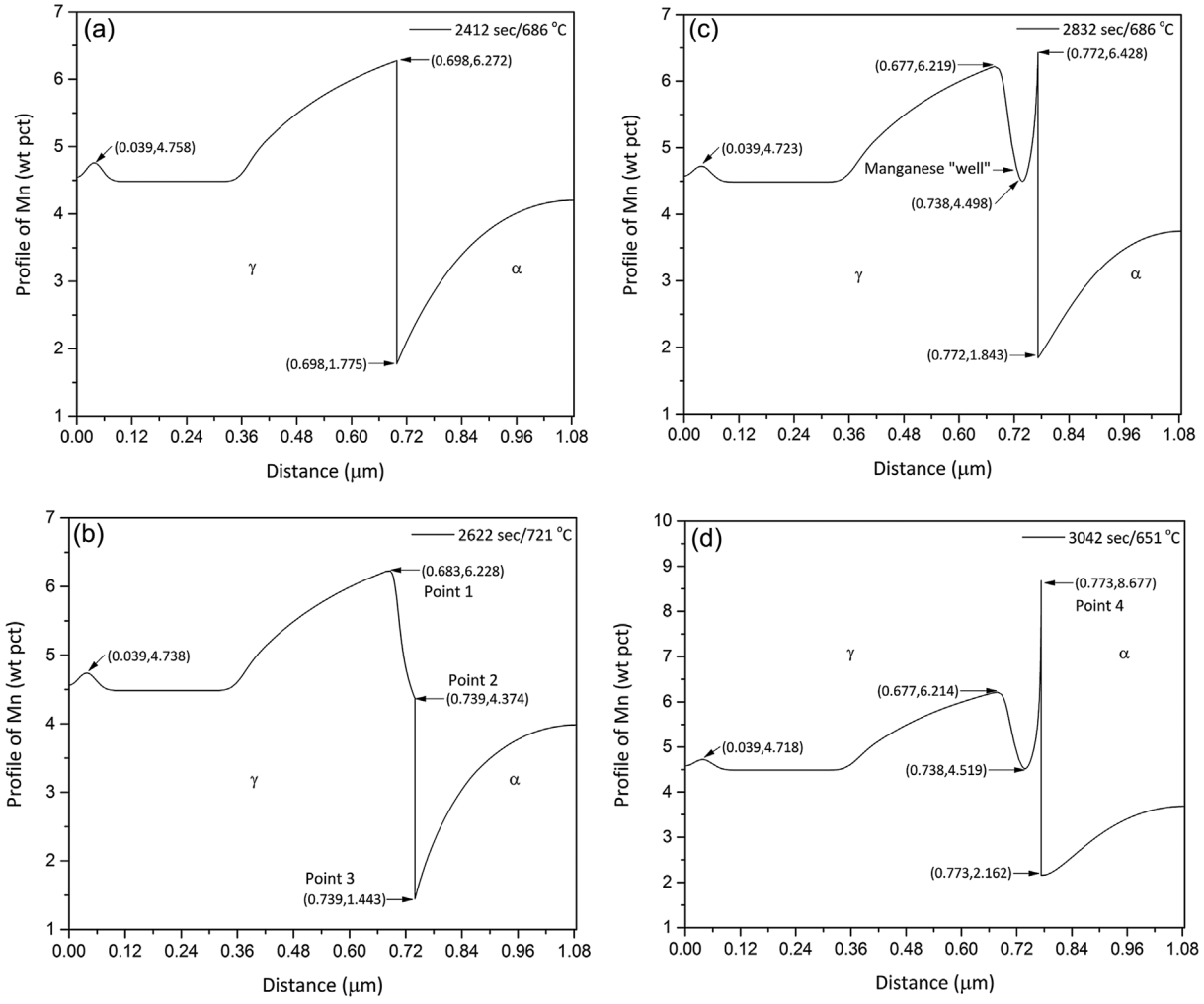

Figure 8. Evolution of the manganese profile during the first cycle of the transformation: a) and b) during heating, c) and d) during cooling, for the times/temperatures indicated. The austenite and ferrite regions are on the left and right of the interface, respectively. The manganese "well" is depicted in c).

proceed forward. The Mn concentration in austenite at the α/γ interface increases and the Mn profile in austenite forms a "well." The "well" corresponds to the locus of the equilibrium Mn composition in austenite at the α/γ interface, as the interfacial compositions change during thermal cycling. During heating, the Mn composition at the interface decreases while during cooling it increases, forming the "well." At T_{min}, a "stagnant" stage is observed where the shift of the interface negligible. Point 4 in Figure 8d corresponds to the Mn composition in austenite at the α/γ interface according to local equilibrium. The same behavior is repeated in the second and third cycles. It is important to note that Mn partitioning follows a similar behavior both during the forward and inverse transformations, i.e., Mn diffuses from ferrite to austenite and the transformation rate is controlled by the Mn diffusion in ferrite.

Carbon exhibits a similar behavior to Mn, although the composition fluctuations are smaller. The evolution of the carbon profiles in the first cycle is depicted in **Figure 9**. A carbon "well" forms in austenite. The compositions of the well correspond to the local equilibrium compositions of carbon in austenite at the α/γ interface, which change during the thermal cycle. In contrast to Mn, the concentration of C in ferrite becomes homogeneous due to the faster diffusion of C in ferrite.

The Mn and C profiles at the end of the third cycle are depicted in **Figure 10**. Three wells have formed corresponding to the three cycles. The Mn "wells" are not homogenized due to the low diffusivity of Mn in austenite. This leads to the formation of a Mn-layered segregation profile, exhibiting maxima and minima in composition, as a result of thermal cycling. The same holds for carbon, although some homogenization is apparent in the time period of the three cycles.

The Mn and C spikes appearing at the start of the isothermal holding, at the location 0.039 μm in Figure 8 and 9, are compositional spikes, which form due to the

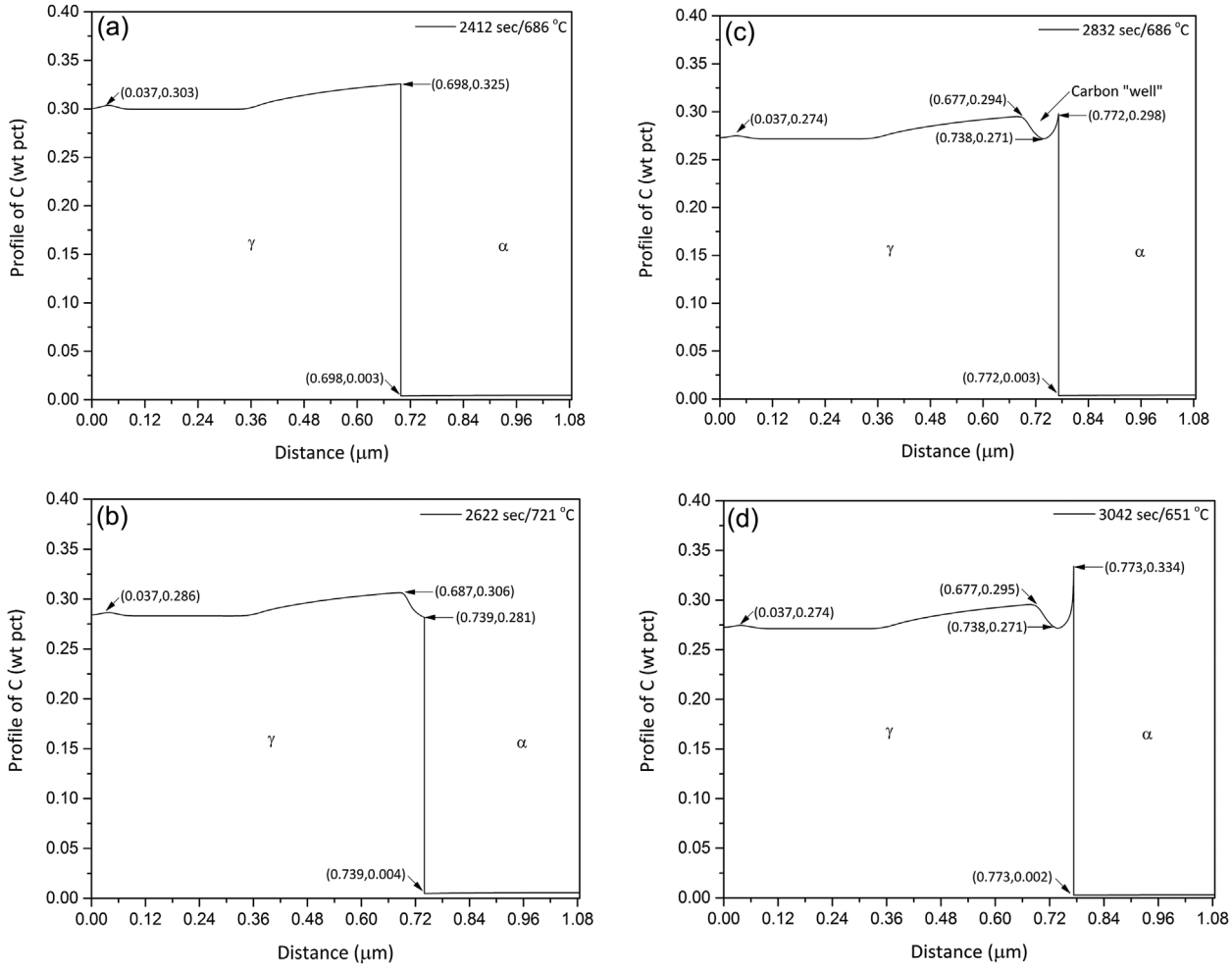

Figure 9. Evolution of the carbon profile during the first cycle of the transformation: a) and b) during heating, c) and d) during cooling, for the times/temperatures indicated. The austenite and ferrite regions are on the left and right of the interface, respectively. The carbon "well" is depicted in c).

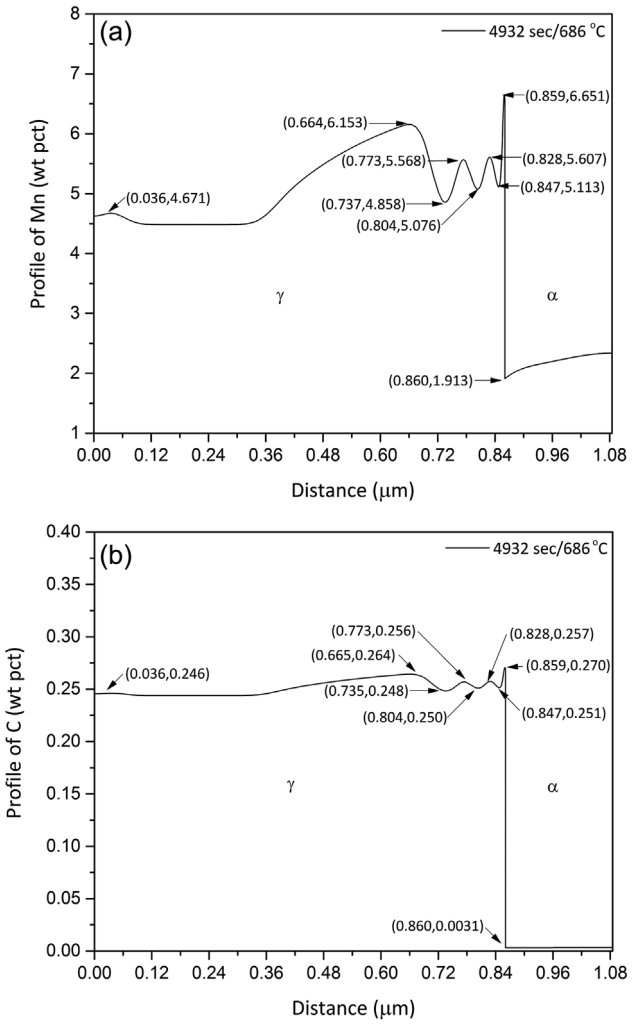

Figure 10. a) Manganese and b) carbon profiles after the three cycles of the cyclic transformation. The formation of three "wells" is indicated.

NPLE conditions prevailing at the beginning of the isothermal transformation. The evolution of these compositional spikes has been described in detail.[21,22]

4. Conclusions

Austenite evolution and solute partitioning during thermal cycling in the intercritical range have been studied for a Fe–0.2C–4.5Mn (mass%) steel for a case where the starting time of the cyclic treatment is well before the equilibrium fractions have been established in the respective isothermal intercritical treatment. From the results of the simulations and experiments, the following conclusions can be drawn:

1. The evolution of austenite during thermal cycling in the intercritical range comprises of forward, inverse, and stagnant stages. The simulation results have been experimentally validated by dilatometry.
2. Austenite formation proceeds with the forward transformation during the heating part and with the inverse transformation during the cooling part of the cycle. Both transformations take place at comparable rates. The fraction of austenite formed decreases in each successive cycle due to a corresponding decrease of the transformation rate.
3. The kinetics of the evolution of austenite during the cyclic transformation is controlled by the Mn diffusion in ferrite, both for the forward and the inverse transformations.
4. Partitioning of Mn and C takes place from ferrite to austenite during the cyclic transformation. Due to the low diffusivity in austenite, wells form in the composition profiles in austenite of both Mn and C. These wells are the locus of the interfacial compositions of austenite corresponding to the variation of the local equilibrium conditions during the thermal cycle.
5. The wells in the composition profiles correspond to the formation of a layered segregation in austenite, exhibiting maxima and minima, as the result of the cyclic thermal treatment in the intercritical range.

Acknowledgements

The work has been conducted in the framework of the IKYDA 2014–2015 program "Design rules for 3rd generation advanced high strength steels," which is a collaboration between the University of Thessaly and RWTH-Aachen.

Received: February 12, 2016; Revised: March 23, 2016

Keywords: cyclic transformations; inverse transformation; austenite

References

[1] D. K. Matlock, J. G. Speer, in *Microstructure and Texture in Steels* (Eds: A. Haldar, S. Suwas, D. Bhattacharje), Springer, London **2009**.
[2] D. K. Matlock, J. G. Speer, E. De Moor, P. J. Gibbs, *JESTECH* **2012**, *15*, 1.
[3] D. W. Suh, J. H. Ryu, M. S. Joo, H. S. Yang, K. Lee, H. K. D. H. Bhadeshia, *Metall. Mater. Trans. A* **2012**, *44*, 286.
[4] S. J. Lee, S. Lee, B. C. De Cooman, *Scr. Mater.* **2011**, *65*, 225.
[5] V. F. Zackay, E. R. Parker, D. Fahr, R. Bush, *Trans. Am. Soc. Met.* **1967**, *60*, 252.
[6] O. Matsumura, Y. Sakuma, H. Takechi, *Trans. ISIJ* **1987**, *27*, 570.
[7] H. Kamoutsi, E. Gioti, G. N. Haidemenopoulos, Z. Cai, H. Ding, *Metall. Mater. Trans. A* **2015**, *46*, 4841.

[8] R. L. Miller, *Metall. Trans.* **1973**, *3*, 905.
[9] D. W. Suh, S. J. Park, T. H. Lee, C. S. Oh, S. J. Kim, *Metall. Mater. Trans. A* **2010**, *41*, 397.
[10] M. J. Merwin, *SAE Technical Paper*, SAE, Warrendale, Pennsylvania **2007**.
[11] H. Huang, O. Matsumura, T. Furukawa, *Mater. Sci. Technol.* **1994**, *10*, 621.
[12] Z. H. Cai, H. Ding, X. Xue, Q. B. Xin, *Mater. Sci. Eng. A* **2013**, *560*, 388.
[13] Z. H. Cai, H. Ding, R. D. K. Misra, H. Kong, H. Y. Wu, *Mater. Sci. Eng. A* **2014**, *595*, 86.
[14] H. Chen, S. van der Zwaag, *Comp. Mater. Sci.* **2010**, *49*, 801.
[15] H. Chen, B. Appolaire, S. van der Zwaag, *Acta Mater.* **2011**, *59*, 6751.
[16] P. I. Sarafoglou, M. I. T. Tzini, G. N. Haidemenopoulos, *Int. J. Met. Mater. Eng.* **2015**, *1*, 104.
[17] J. O. Anderson, T. Helander, L. Höglund, P. Shi, B. Sundman, *Calphad* **2002**, *26*, 273.
[18] A. Borgenstam, L. Hoglund, J. Agren, A. Engstrom, *J. Phase Equilb.* **2000**, *21*, 269.
[19] R. Wei, M. Enomoto, R. Hadian, H. S. Zurob, G. R. Purdy, *Acta Mater.* **2013**, *61*, 697.
[20] N. Nakada, K. Mizutani, T. Tsuchiyama, S. Takaki, *Acta Mater.* **2014**, *65*, 251.
[21] M. Hillert, *Metall. Trans. A* **1984**, *15A*, 141.
[22] H. Chen, K. Zhu, L. Zhao, S. van der Zwaag, *Acta Mater.* **2013**, *61*, 5458.